Efficient New Numerical Technique for RC Structures with Construction Defects under Monotonic and Cyclic Loading Conditions

Mostafa Fahim[1], Said Elkoly[2] and Shreif Morad[3]

***Abstract*— Forms in concrete construction are vital as they provide the fresh concrete its shape and hold it until it hardens. Concrete compaction may not be required if self-compacting concrete (SCC) is the construction material used. After removal of the forms, concrete which is honeycombed should be repaired, or replaced, prior to the application of curing compound. But some contractors repair honeycombed concrete at the end of the construction. The consequences of doing so will affect the long-term properties of the honeycombed members and may be serious if the building is hit by an unexpected load such as earthquake during construction. In this study a finite element (FE) model is proposed and utilized in the analysis of reinforced concrete columns with honeycomb defects and subjected to gravity and horizontal loads. The FE program developed is based on the fiber beam-column element technique. The outcomes of the developed FE program were verified and compared to those of experimental test results in the literature. A parametric study was performed to investigate the effects of different parameters that may affect the lateral load resistance of RC-columns such as honeycomb location, size, depth and loading factor. The results show that the location and loading factor (applied vertical load) have significant influence on the lateral load resistance of the RC columns.**

Keywords: Cyclic loading, Fiber element model, Honeycomb defects, RC columns.

I. Introduction

CONSTRUCTION defects are a significant source of maintenance costs. Faulty construction is one of the most common causes of early deterioration. Common construction faults include inadequate compaction and failure to the place of reinforcement resulting in inadequate concrete cover Zietsman, [1]. Based on the survey of building failure patterns and their implications conducted by The Building Research Establishment in the United Kingdom (UK) to determine the most common defects, it was found that 35% of the defects were originated from faulty construction (Assaf, Al-Hamad, Al-Shihah, [2]). One of the common construction defects is honeycombing. Honeycombs are construction defects caused by improper vibration during concrete placement, resulting in the segregation of the coarse aggregates from the fine aggregates and cement paste. It may also occur due to excessive mixing of the concrete and low workability of the concrete. In some cases, honeycombs are the result of insufficient vibration, where the entire concrete mix does not physically reach the formwork surface (Figure 1). Severe honeycombs, which are also known as rock pockets, occur when an excessive amount of aggregate is found without the presence of cement paste.

According to most of the construction and design codes and repair standards (such as ACI 301, [3] and ACI 503.4, [4]), repair of surface defects shall begin immediately after form removal. Segregation, which corresponds to the loss of homogeneity between both the granular and the suspending phases (Bethmont, et al. [5]), remains one of the major problems of both traditional and self-compacting concretes. Consequences of this pathology are numerous and may affect the long-term properties of the structures (resistance, durability).

Figure 1 Concrete Honeycomb

In order to evaluate influence of honeycombs on the ultimate resistance of RC structures due to honeycombs, detailed three dimensional-nonlinear-finite-element analysis provides an accurate alternative. However using this type of analysis is relatively complex and increases the modeling and computing times. In this paper an alternative numerical technique based on fiber element model is developed to facilitate the simulation of reinforced concrete that has construction defects such as honeycombs under monotonic static and cyclic loading conditions. After developing the new technique, a

Manuscript received December 11, 2012.

[1] Ph.D Candidate, Faculty of Engineering, Cairo University, Giza, Egypt, E-mail: mostafa.fahim@gmail.com

[2] Associate Professor of Structural Engineering, Faculty of Engineering, Fayoum University, Fayoum , Egypt,E-mail: sak00@fayoum.edu.eg

[3] Professor of Structural Engineering, Faculty of Engineering, Cairo University, Giza, Egypt, E-mail: smourad2006@gmail.com.

detailed evaluation is carried out by comparing its results to the available experimental results. The capability of the proposed numerical approach to predict the experimentally observed load–displacement response, strain distributions is verified. The proposed method provides the best compromise between simplicity and accuracy in nonlinear analysis of concrete structures with defected members. Finally, a detailed sensitivity analysis is performed to evaluate the influence of different aspects that control the performance of RC columns defected by honeycombs

II. FIBER ELEMENT MODEL

Material nonlinearity in a frame element is commonly described by either lumped or distributed plasticity models. In the lumped plasticity models, a frame element consists of two zero-length nonlinear rotational spring elements and an elastic element connecting them. The nonlinear behavior of a structure is captured by the nonlinear moment–rotation relationships of these spring elements. Due to the simplicity of the formulation, the lumped plasticity model is widely used when the computational cost of the analysis is high, e.g. in the case of nonlinear time-history analysis of a large structure. Most lumped models, however, oversimplify certain important aspects of the hysteretic behavior of reinforced concrete members and are, therefore, limited in applicability. One such limitation derives from restrictive a priori assumptions for the determination of the spring parameters. Parametric and theoretical studies of girders under monotonic loading presented by Anagnostopoulos [6], demonstrate a strong dependence between model parameters and the imposed loading pattern and level of inelastic deformation. Neither factor is likely to remain constant during the dynamic response. The problem is further accentuated by the fluctuation of the axial force in the columns. Because of this history dependence, damage predictions at the global, but particularly at the local level, may be grossly inaccurate. Another limitation of most lumped plasticity models proposed to date is their inability to describe adequately the deformation softening behavior of reinforced concrete members. Such deformation softening can be observed as the reduction in lateral resistance of an axially loaded cantilever column under monotonically increasing lateral tip displacement (Taucer, et al. [7]).

This study proposes a new fiber beam-column finite element model coupled with a consistent nonlinear solution algorithm using Object Orientated Programming (OOP). The proposed method is particularly suitable for the analysis of the highly nonlinear hysteretic behavior of RC columns under varying axial and lateral loads. There are several advantages which justify the use of fiber analysis. Some of these advantages include but are not limited to their ability to handle, Perea and Leon [8]:

• Complex cross-sections: A fiber cross-section can have any general geometric configuration formed by sub-regions of simpler shapes; geometric properties are calculated through the numerical integration.

• Tapered elements: Since the length of the fiber is not considered, the cross-section defined at each of the two ends can be different, and therefore, the response can be roughly estimated. Precision can be increased with more integration points.

• Complex strength-strain behavior: Since each fiber can have any stress-strain response, this technique allows modeling nonlinear behavior in steel, reinforced concrete and composite structures.

• Accuracy and efficiency: Since each fiber is associated to a given uniaxial stress-strain (s-e) material response, higher accuracy and more realistic behavior effects can be captured in a fiber-based model than in a frame-based model, and at less computing time than for a 3D finite-based model.

• The major advantages of using OOP in programming are simplicity, modifiability, extensibility, re-usability etc.

The fiber beam-column finite element models for the nonlinear analysis of reinforced concrete members are, presently, flexibility-based fiber element models. In these models the element is subdivided into longitudinal fibers, as shown in Figure 2. The geometric characteristics of the fiber are its location in the local y, z reference system and the fiber area.

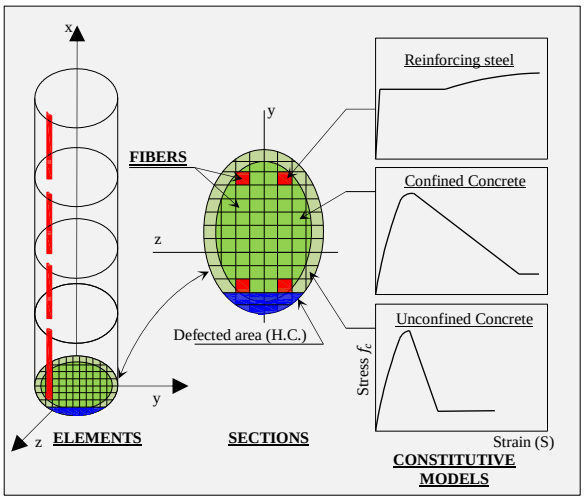

Figure 2 Fiber element distribution of control sections and section subdivision into fibers

The constitutive relation of the section is not specified explicitly, but is derived by integration of the response of the fibers, which follow the uniaxial stress-strain relation of the particular material. The elements proposed to date are limited to small displacements and deformations.

A. FIBER CONSTITUTIVE MODELS

Reinforced concrete structures are made of up to two materials with different characteristics, namely, concrete and steel reinforcement. The nonlinear behavior of these materials is caused by two major effects, namely, cracking and/or crushing of concrete in tension and compression, respectively, and yielding of the reinforcement steel bars. In the following

subsections the behavior of each constituent material and the derivation of the corresponding material stiffness matrix are discussed.

• *Concrete Stress-Strain*

Hysteretic constitutive laws for confined and unconfined concrete and for steel are incorporated in the model to define the stiffness and strength properties of the fiber beam-column elements. In this study, the monotonic envelope curve of concrete in compression follows the model of the modified Kent and Park model, Park, et al. [9]. The implemented concrete model describes the concrete stress-strain relation under an arbitrary cyclic strain history. Four important factors were taken into account:

- The most significant parameter affecting the shape of the stress-strain curve of confined concrete for all section shapes was the quantity of confining reinforcement, Mander, et al. [10].
- The successive degradation of stiffness of both the unloading and reloading curves, for increasing values of compressive strain.
- The effect of tension stiffening.
- The hysteretic response under cyclic loading in compression.

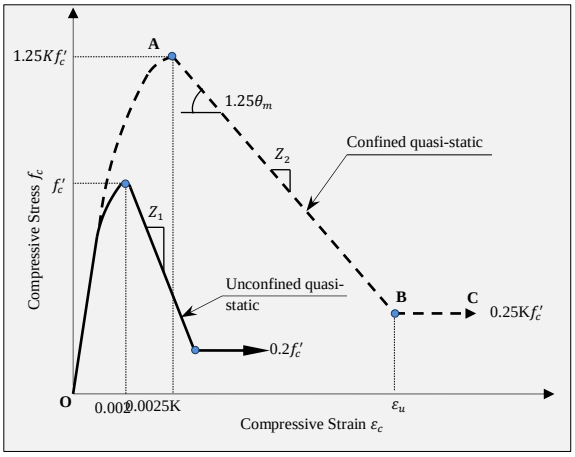

Figure 3 Modified Kent and Park Model for Concrete

The original Kent and Park stress-strain model for concrete confined by rectangular hoops without supplementary cross ties was proposed based on the experimental data obtained by Roy and Sozen, Bertero and Felipa, and Soliman and Yu, Sheikh [11]. In the study by Park et al. [9] where four full size reinforced concrete columns confined by rectangular hoops with supplementary cross ties were tested under combined axial load and flexure, strength enhancement of core concrete was evident. Consequently, they proposed a modified form of the original Kent and Park model taking into account the strength enhancement and increase of strain at maximum stress of confined core concrete, as illustrated in Figure 3.

In the modified Kent and Park model it is assumed that the maximum stress, Kfc' is reached at a strain of εo=0.0025K. The monotonic concrete stress-strain relation in compression is described by three regions (Yassin [12]) as follows:

For $\varepsilon_c \le \varepsilon_o$ (Region OA)

$$f_c = Kf_c'\left[\frac{2\varepsilon_c}{0.002K} - \left(\frac{\varepsilon_c}{0.002K}\right)^2\right] \quad (1)$$

For $\varepsilon_o < \varepsilon_c \le \varepsilon_{20}$ (Region AB)

$$f_c = Kf_c'[1 - Z_m(\varepsilon_c - 0.002K)] \prec 0.2Kf_c' \quad (2)$$

For $\varepsilon_c > \varepsilon_{20}$ (Region BC)

$$f_c = 0.2Kf_c' \quad (3)$$

where

$$Z_m = \frac{0.5F_D}{\left[\frac{3 + 0.29f_c'}{145f_c' - 1000}\right] + 0.75\rho_s\sqrt{\frac{h}{s_h}} - 0.002K}$$

$$\varepsilon_o = 0.002K$$

$$K = F_D\left[1 + \rho_s f_{yh}/f_c'\right]$$

f_c' Concrete compressive cylinder strength in MPa
Z_m The strain softening slope
ε_{20} The concrete strain at 20 percent of maximum stress
F_D The strain-rate dependent constant taken as 1.0 for low rates
K Confinement coefficient
f_{yh} Yield strength of stirrups in MPa
ρ_s Ratio of the volume of hoop reinforcement to the volume of concrete core measured to outside of stirrups
h Width of concrete core measured to outside of stirrups
s_h Center to center spacing of stirrups or hoop sets

Various stress–strain models for the prediction of the confined concrete have been proposed. Almost all analytical models were developed on the basis of the observations in the experimental studies, Bousalem and Chikh [13]. In this study, the mathematical model used to describe the cyclic loading curve was constructed from the modified Kent and Park that takes into account concrete tensile strength, concrete damage and hysteresis, while retaining computational efficiency.

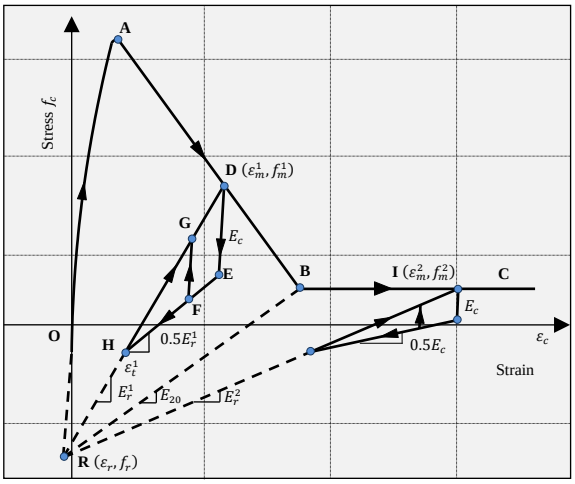

Figure 4 Concrete Material Model under Cyclic Loading in Compression

Figure 4 shows the compressive behavior of the model. There is a successive degradation of stiffness of both the unloading and reloading lines, for increasing values of the maximum strain. The degradation of stiffness is such that the projections of all reloading lines intersect at a common point R. Point R is determined by the intersection of the tangent to the monotonic envelope curve at the origin and the projection of the unloading line from point B that corresponds to a concrete strength of $0.2f_c'$. The strain and stress at the intersection point are given by the following expressions,

$$\varepsilon_r = (0.2Kf_c' - E_{20}\varepsilon_{20})/(E_c - E_{20}) \quad (4)$$

$$f_r = E_c\varepsilon_r \quad (5)$$

After unloading from a point on the compressive monotonic envelope (point D in Figure 4), and before reaching the zero stress axis (point H in Figure 4), the model response follows two smaller envelopes that are defined by the following equations:

$$\text{Line HD - } f_{max} = f_m + E_r.(\varepsilon_c - \varepsilon_m) \quad (6)$$

$$\text{Line HE - } f_{min} = 0.5E_r.(\varepsilon_c - \varepsilon_t) \quad (7)$$

where

$$E_r = (f_m - f_r)/(\varepsilon_m - \varepsilon_r)$$

$$\varepsilon_t = \varepsilon_m - (f_m/E_r)$$

Therefore, the positions of the two smaller envelopes depend on the position of the unloading point. For partial loading and unloading cycles within the smaller envelopes the model follows a straight line with modulus E_c in the numerical implementation a trial stress and tangent modulus is assumed based on linear elastic behavior with slope E_c :

$$f_c^t = f_c' + E_c.\Delta\varepsilon_c \quad (8)$$

where

f_c^t The new trial stress
f_c' The previous stress state
$\Delta\varepsilon_c$ The strain increment

The following rules are then used to determine actual stress and modulus of the model.

$$\text{If } f_{min} \le f_c^t \le f_{max} \text{ then}$$
$$f_c = f_c^T \text{ and } E_t = E_c \quad (9)$$

$$\text{If } f_c^t < f_{min} \text{ then}$$
$$f_c = f_{min} \text{ and } E_t = 0.5E_r \quad (10)$$

$$\text{If } f_c^T > f_{max} \text{ then}$$
$$f_c = f_{max} \text{ and } E_t = E_r \quad (11)$$

If unloading occurs from point D to point E, reloading will be on the same path back to D. If unloading reaches point F, the hysteresis loop DEFGD will result upon reloading. If complete unloading to point H occurs, reloading will result in the hysteresis loop DEHD. It is important to note that the reloading line will always rejoin the compression monotonic envelope at the point of initial unloading. For the case when unloading continues past point H and the model starts reloading in tension, a different set of rules governs the hysteretic behavior.

The tensile behavior of the model, as shown in Figure 5, takes into account tension stiffening and the degradation of the unloading and reloading stiffness for increasing values of maximum tensile strain after initial cracking. The maximum tensile strength of the concrete (modulus of rupture) is assumed equal to:

$$f_t' = 0.6228\sqrt{f_c'} \quad (12)$$

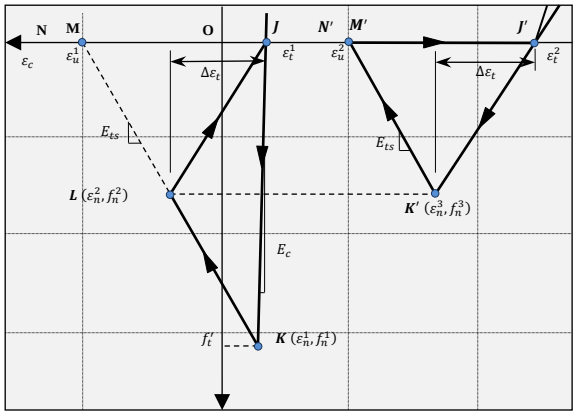

Figure 5 Concrete Material Model Under Cyclic Loading in Tension

Figure 5 shows two consecutive tensile hysteresis loops which are part of a sample cyclic history that also includes compressive stresses.

The model assumes that tensile stress can occur anywhere along the strain axis, either as a result of initial tensile loading

or as a result of unloading from a compressive state. In the latter case a tensile stress occurs under a compressive strain. The tensile stress-strain relation is defined by three points with coordinates $(\varepsilon_t, 0)$, (ε_n, f_n), $(\varepsilon_u, 0)$ as represented by points J, K and M shown in Figure 5. ε_t is the strain at the point where the unloading line from the compressive stress region crosses the strain axis. ε_t is given by Equation (13) and changes with the maximum compressive strain. ε_n and f_n are the strain and stress at the peak of the tensile stress-strain relation and are given by the following expressions:

$$\varepsilon_n = \varepsilon_t + \Delta\varepsilon_t. \quad (13)$$

$$f_n = f_t' + (1 + E_{ts}/E_s) - E_{ts}\Delta\varepsilon_t \quad (14)$$

where

$\Delta\varepsilon_t$ The previous maximum differential between tensile strains (f_t'/E_c)

ε_t As shown in Figure 5 the strain before initial cracking

E_{ts} The tension stiffening modulus that depends on numerical and physical parameters

ε_u The strain at the point where the tensile stress is reduced to zero and is given by the expression

$$\varepsilon_u = \varepsilon_t + f_t'.(1/E_{ts} + 1/E_c) \quad (15)$$

Given these three control points, the tensile stress-strain relation and tangent modules are defined by the following equations (tension is positive):

Region JK: $\varepsilon_t < \varepsilon_c \le \varepsilon_n$

$$f_c = E_t(\varepsilon_c - \varepsilon_t),\ E_t = f_n/(\varepsilon_n - \varepsilon_t) \quad (16)$$

Region KM: $\varepsilon_n < \varepsilon_c \le \varepsilon_u$

$$f_c = f_n + E_t(\varepsilon_c - \varepsilon_n),\ E_t = -E_{ts} \quad (17)$$

Region MN: $\varepsilon_c > \varepsilon_u$

$$f_c = 0,\ E_t = 0 \quad (18)$$

If $\varepsilon_n \ge \varepsilon_u$ then f_n, f_c and E_t are all assumed to be zero. The modulus E_{ts} controls the degree of tension stiffening by controlling the slope of Equation (16). The steeper the slope, the smaller the effect of tension stiffening will be. Tensile unloading and reloading are governed by Equation (15) which also includes stiffness degradation for increasing values of the strain differential $\Delta\varepsilon_t$. The value of $\Delta\varepsilon_t$ changes whenever $\varepsilon_c > \varepsilon_n$

.

- *Steel Stress-Strain*

In this research, one of the most accurate models of a stress-strain relationship of the steel material is adapted to simulate the following characteristics which are shown in Figure 6.

The Giuffre-Menegotto-Pinto model was initially proposed by Giuffre and Pinto and later used by Menegotto and Pinto, Gomes and Appleton [14]. The loading and unloading paths are contained in a bilinear envelope defined by

$$f_s = E_\infty\varepsilon_s + \frac{(E_{s0} - E_\infty)\varepsilon_s}{(1 + (\varepsilon_s/\varepsilon_0)^R)^{1/R}} \quad (19)$$

This equation represents a curve with a tangent at the origin:

$$f_s = E_{s0}\varepsilon_s \quad (20)$$

And with a straight line asymptote for $\varepsilon_s \to \infty$

$$f_s = E_\infty\varepsilon_s + (E_{s0} - E_\infty) \quad (21)$$

where

E_{s0} Initial tangent modulus of the stress-strain curve

E_∞ Secondary tangent modulus (for large strain)

R Constant taking into account the Baushinger effect

ε_0 f_0/E_{s0} Strain at the intersection point between the tangent at the origin and the asymptote.

f_s, ε_0 Engineering stress and strain, respectively

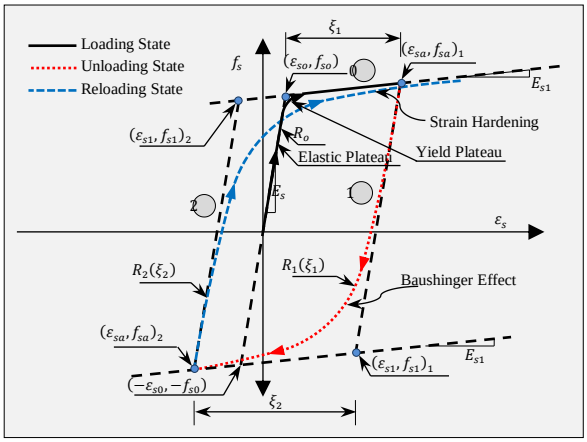

Figure 6 Reinforcement Bars Material Model under Cyclic Loading

The Menegotto-Pinto model has two distinct advantages with respect to the implicit Ramberg-Osgood law, Albensi and Nuti [15] . First, each parameter (E_0, E_∞, f_0, ε_0, R) in Equation. (19) defines a separate aspect of the curve geometry, so these can be manipulated independently and easily identified on an experimental diagram. Second, good initial estimates for the three out of the four independent parameters (note that $f_0 = E_0\varepsilon_0$) can be obtained by taking measurement directly from the experimental curve.

Equation (19) can be written in a dimensional form also useful to describe the cyclic response:

$$f_s^* = \beta\varepsilon_s^* + (1 - \beta)\frac{\varepsilon_s}{(1 + (\varepsilon_s^*)^R)^{1/R}} \quad (22)$$

The normalized strain and stress ε_s^*, f_s^* are obtained by a variable substitution given in the first loading curve, by

$$\varepsilon_s^* = \frac{\varepsilon_s}{\varepsilon_{so}} \quad \& \quad f_s^* = \frac{f_s}{f_{so}}$$

And after the load reverse by

$$\varepsilon_s^* = \frac{\varepsilon_s - \varepsilon_{sa}}{2\varepsilon_{so}} \quad \& \quad f_s^* = \frac{f_s - f_{sa}}{2f_{so}}$$

where

ε_{so}, f_{so} Strain and stress, respectively, at the yield point

ε_{so}, f_{so} Strain and stress, respectively, at the yield point

ε_{sa}, f_{sa} Strain and stress, respectively, at the inversion point in Figure 6.

$\beta = E_{sh}/E_s$ Ratio between the hardening stiffness, E_{sh} and the tangent modulus of elasticity at the origin, E_s

R Constant taking into account the Baushinger effect

Equation (21) represents a curved transition from a straight line asymptote with a slope E_s beginning at $(\varepsilon_{sa}, f_{sa})$ to another asymptote with a slope E_{sh} . The distance to the elastic curve, which simulates the Baushinger effect, is a function of the parameter R defined by $R = R_o - \frac{a_1 \xi}{a_2 + \xi}$

Where R_o, a_1, a_2 are material constants. Recommended values are $R_o =$ between 10 and 20, $a_1 = 0.925$, $a_2 = 0.15$. ξ : is the absolute value of the plastic strain of the last excursion in Figure 6

To simulate the isotropic strain hardening, Filippou, et al. [16], have proposed two modifications of this model. The first one consists of a new variable substitution defined by

$$\varepsilon_s^* = \frac{\varepsilon_s - \varepsilon_{sa}}{\varepsilon_{s1} - \varepsilon_{sa}} \quad (23)$$

$$f_s^* = \frac{f_s - f_{sa}}{f_{s1} - f_{sa}} \quad (24)$$

where: ε_s^*, f_s^* are the strain and stress, respectively, of the intercession point of the envelope line to the elastic path.

As indicated in Figure 6, this modification has the objective of improving the accuracy of the model. The other modification consists in the change of the yield stress value to take into account the isotropic strain hardening. After a load reversal the yield stress, f_{so}^e, that defines the hardening envelope line, is given by

$$f_{so}^e = f_{so} a_3 \left(\frac{\varepsilon_{smax}}{\varepsilon_{so}} - a_4 \right) \quad (25)$$

where ε_{smax} is the maximum absolute strain value before the load reverse and a_3 , a_4 are constants of the material.

• *Beam-Column Element Formulation*

The basic assumption in a flexibility-based model is that the internal force distribution in the element is in a consistent state determination process, the section forces are determined from the element forces, followed by the computation of the corresponding fiber stresses based on equilibrium. The fiber strains and flexibilities are determined from the fiber stress-strain relations and the section deformations.

The determination of fiber stresses from section forces is, however, a statically indeterminate problem for a section with more than two fibers: the fiber stresses cannot be determined from the axial force and bending moment at the section, since there are only two equilibrium equations in the uniaxial bending. One possible solution is to assume a stress distribution within the section, but the problem is, then, only postponed to the fiber state determination phase of the algorithm, since fiber stress-strain relations are typically expressed as explicit functions of strain, Berry, et al. [17]. The solution adopted in the proposed models is to linearize the section constitutive relation and compute the section deformations from the new section forces and the section flexibility from the previous step. Fiber stresses and stiffnesses are then determined from the fiber stress-strain relations. The section resisting forces are computed from the fiber stress distribution and the section stiffness k(x) is assembled from the fiber stiffnesses. In the uniaxial bending case k(x) takes the form

$$k(x) = \begin{bmatrix} \sum_{i=1}^{n(x)} E_i . A_i & -\sum_{i=1}^{n(x)} E_i . A_i . y_i \\ -\sum_{i=1}^{n(x)} E_i . A_i . y_i & \sum_{i=1}^{n(x)} E_i . A_i . y_i^2 \end{bmatrix} \quad (26)$$

The section stiffness is then inverted to yield the section flexibility f(x)= (k^{-1}) (x). The new element flexibility F is computed and is then inverted to obtain the element stiffness k=F−1. The remaining problem is the determination of the element resisting forces from the section resisting forces along the element. The nonlinear solution Algorithm is presented below step by step. The solution focuses on a single iteration;

Solve the global system of equations and update the structural displacements.
Calculate the element deformation increments and update the element deformations.
Start the element state determination. Loop over all elements in the structure.
Determine the element force increments.
Update the element forces.
Determine the section force increments. Steps (6) through (11) are performed for all control sections (integration points) of the element.
Determine the section deformation increments.
Determine the tangent stiffness and flexibility matrices of the section.
Determine the section resisting forces.
Determine the unbalanced forces at the section.
Determine the residual section deformations.
Determine the element flexibility and stiffness matrices.
Check for element convergence.
Determine the resisting forces and the new stiffness matrix of the entire structure.

• Scope of the method and limitations

The scope of this paper is limited to studying the effect of honeycombs on the behavior of reinforced concrete columns. The formulation of the fiber beam-column element is based on the assumption that the element has linear geometry. Plane sections remain plane and normal to the longitudinal axis during the element deformation history.

Shear effects are ignored, which is a reasonable approximation for medium to large span to depth ratios of the member.
The proposed element does not account for deformations due to shear and torsion.

• Comparison with Experimental Data

To evaluate the reliability and the accuracy of the developed technique, several numerical examples were developed and compared with the corresponding experimental tests' results under monotonic static as well as cyclic loading conditions. for sake of brifity, only one of those models is presented.

Figure 7 shows the concrete dimensions and the reinforcement details of one of the benchmark experimental test done by Ohno and Nishioka [14]. Five cantilevered columns were tested under constant axial load and cyclic lateral load. The variables studied were the lateral load pattern and the level of axial load. The lateral load pattern for the test specimen is shown in Figure 8. Two load cycles are applied to the column in Figure 9 shows comparisons between the horizontal load versus the horizontal displacement relationship obtained from the introduced technique and the experimental results of column L1. From the figure, it is clear that the behavior is well predicted in the elastic stage, post cracking stage, and in the post-yielding stage.

As it can be observed the hysteresis loops predicted by the proposed model are closer to the experimental results at every point and the error in unloading branch area for the first loop was the highest but it decreased in the second loop and still less than 5 percent and less than 1 percent for the other areas The proposed model shows a very good agreement with the experimental results.

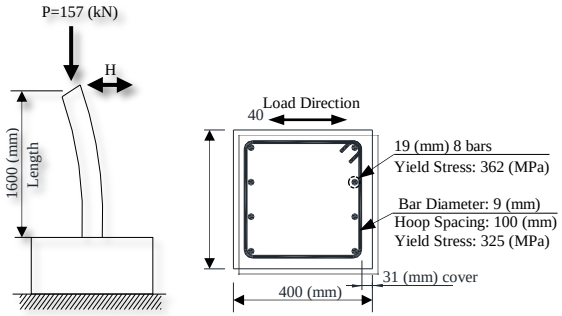

Figure 7 Loading sub-Assemblage & Section Properties

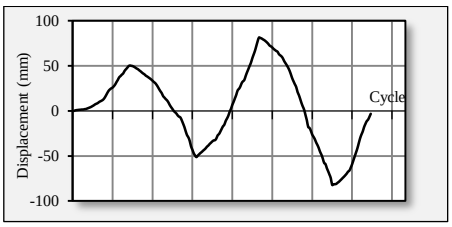

Figure 8 Loading Hysteresis for Specimen L1

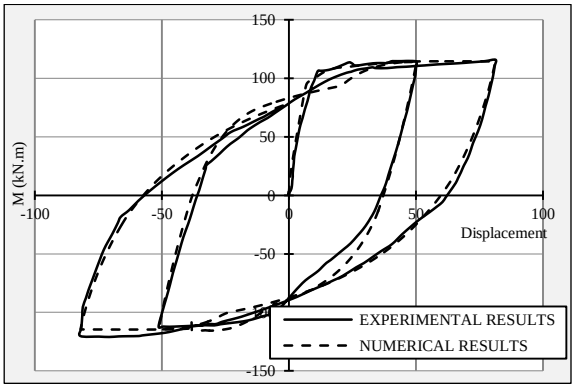

Figure 9 Hysteresis behavior for specimen L1 compared with numerical results

III. CASE STUDY EFFECT OF HONEYCOMB

The main goal of this paper is to assess the performance of RC columns with a construction defect due to honeycomb. To achieve this goal six models representing columns with different sized honeycombs are developed. The honeycomb dimensions various in width (20%, 60%, 100% from total width) and depth (20%, 30% from total depth) as shown in Figure 9. A model for the sound column without honeycomb is also developed to be used as a reference structure. Several factors that influence the performance of the defected column such as honeycomb location, size, amount of axial load and lateral load direction were investigated. The impact of the latter factors will be discussed in the subsequent sections.

• Honeycomb Location

A series of non-linear static push-over analyses were performed using the developed program in order to investigate the influence of the honeycomb location (i.e. height from the column base). A number of analyses were performed changing the height of the honeycomb to evaluate its effect on the lateral load carrying capacity of the column. Based on the numerical output it was found out that the highest change in the lateral capacity occurred when the honeycomb's height is zero, i.e. the honeycomb is at the column base. As the height of the honeycomb increases the influence of the honeycomb drastically reduces. It is noteworthy that the most commonly observed honeycomb occurrence is at the lowest end of the column. Therefore, in all subsequent analyses the location of the honeycomb is set to be zero.

• Effect of Applied Axial Load

While it is recommend to repair the honeycomb defected columns once they are observed, the decision of repairing such columns in many non-engineering buildings is delayed till finishing the construction of the skeleton structure. Therefore, their applied vertical load increases on the defected columns.

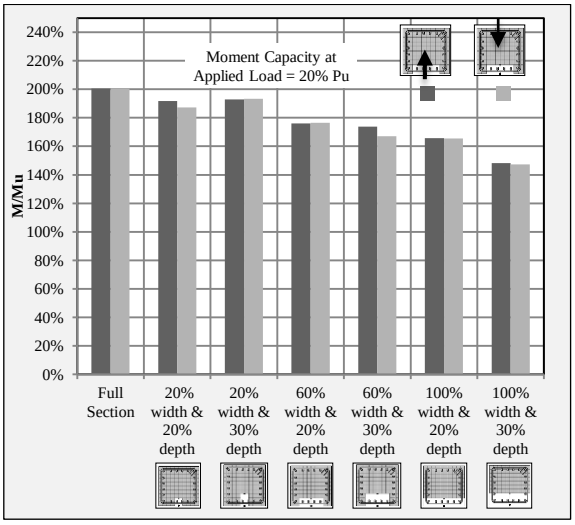

Figure 10 effects of honeycombs on lateral capacity of the column at Pu = 20%

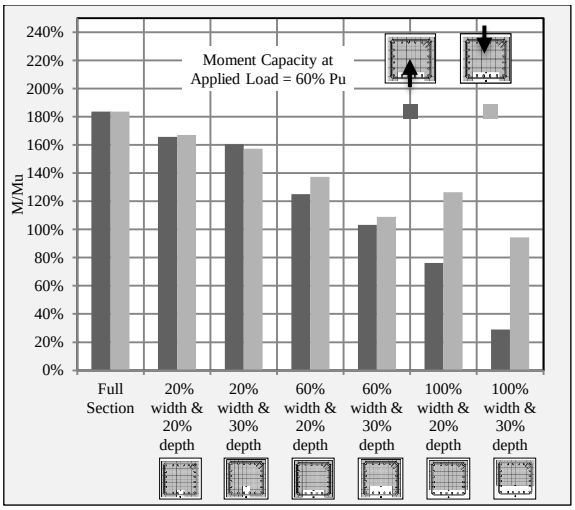

Figure 11 Effects of honeycombs on lateral capacity of the column at Pu = 60%

To assess the effect of the applied axial load on the lateral capacity of columns with honeycombs a series of monotonic non-linear push-over analyses are performed. For the sake of brevity, the results of two cases are presented as shown in Figure 10 and Figure 11.

Two lateral loading directions are used in the analysis, i.e. loading from the face of the column having a honeycomb and the opposite to it. The results are compared with the ultimate load and moment capacity of the sound column. From the Figure (11), it can be shown that the lateral moment capacity of the columns with honeycomb decreases with increasing the honeycomb size. The difference between the lateral capacity in the two loading cases increases by increasing the vertical applied load ratio. Finally, the size of the honeycomb also has a predominant influence on the lateral moment capacity of the columns. For instance, when the widths of the honeycomb equal 100% of the column width and its depth is 20% of the column depth the lateral capacity decreases by approximately 20% of sound column ultimate capacity and by approximately 50% when the ultimate axial load is increased by 60%.

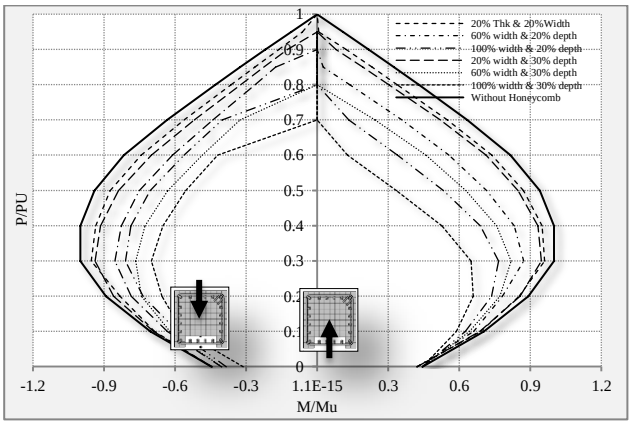

Figure 12 Interaction diagrams of columns defected by honeycombs

Figure 12 summarizes all numerical results obtained using hundreds of runs of the models under different axial loading ratios. The ultimate moment and the corresponding maximum applied load at each point are plotted in interaction diagram envelope.

Table 1 Ductility factor in case of displacement direction is in the direction of honeycomb location

Sections	$P= Pu_{20\%}$	$P= Pu_{60\%}$	$\Delta P = P_{20\%} - P_{60\%}$
Full section (without Honeycomb)	1.96	1.43	0.53
H.C. (20% depth, 20% width)	1.85	1.27	0.57
H.C. (20% depth, 60% width)	1.52	1.05	0.48
H.C. (20% depth, 100% width)	1.56	1.00	0.55
H.C. (30% depth, 20% width)	1.77	1.19	0.58
H.C. (30% depth, 60% width)	1.35	0.81	0.54
H.C. (30% depth, 100% width)	1.45	0.74	0.71

The curve shows that increasing the honeycomb area decreases both axial and lateral load carrying capacity of the columns. Moreover, the curve illustrates that the loading capacity is highly influenced by the lateral loading direction. Finally, the adequate and fast repair is highly required due to high reduction in column lateral capacity by increasing the vertical applied load.

The ductility is defined as the ratio of ultimate displacement over yield displacement. The ultimate displacement (δ_u) is defined as the point that the load is going to decrease. For the case of column under high axial load, the ultimate displacement is still defined as the point that the load start to incline. The yield displacement (δ_y) is defined as displacement at which the reinforcement steel fiber strain reaches the yielding strain.

Table 2 Ductility factor in case of displacement direction is in opposite direction of honeycomb location

Sections	$P = Pu_{20\%}$	$P = Pu_{60\%}$	$\Delta P = P_{20\%} - P_{60\%}$
Full section (without Honeycomb)	1.96	1.43	0.53
H.C. (20% depth, 20% width)	1.89	1.26	0.62
H.C. (20% depth, 60% width)	1.68	0.95	0.73
H.C. (20% depth, 100% width)	1.42	0.65	0.77
H.C. (30% depth, 20% width)	1.81	1.22	0.60
H.C. (30% depth, 60% width)	1.51	0.81	0.70
H.C. (30% depth, 100% width)	1.24	0.35	0.89

Table 1 and Table 2 show the reduction in the columns ductility due to honeycombs. It was found that the ductility reduction is approximately constant and equal to 0.55 (except, the ductility reduction increased to 0.71 in the last honeycomb section) in case the displacement direction is in the same direction of honeycomb location. It was found that the ductility reduced linearly with honeycomb area increased in case of the displacement direction is in the opposite direction of honeycomb location Table 2. Again it can be conclude that the reduction in columns ductility is governed by the following aspects: honeycombs size; loading direction and the axial applied load ratio.

Therefore immediate and adequate repair to honeycombs defected columns is highly recommended specially in moderate and high seismic area zones to avoid structural collapse of the vertical load carrying members during construction.

IV. Conclusion

As described previously, fiber and finite element analysis analyses are very useful techniques to predict the overall behavior of beam-column elements. However, the accuracy on the results is highly dependable on the stress-strain model coupled to the fibers. Figure 9 shows the experimental data compared to the hysteretic loops predicted by the proposed model.

Simple stress-strain models predict reasonably the ultimate strength; however, more complex material models should be assumed to predict ductility and high displacements such that damage is considered. On the other hand, most of the nonlinearity sources (like strength/stiffness degradation, confinement, local buckling and tri-axial stresses effects) have to be calibrated with experimental results and/or more complex analytical techniques in order to incorporate them later on in the uniaxial stress-strain used in the fiber-based model.

The paper highlights the importance of adequate and immediate repair of the defected area with honeycomb especially in moderate and high seismic zones.

The work in this paper was limited to investigating the effects of honeycombs on the performance of reinforced concrete columns under lateral cycling loading condition. Further work is needed to examine the effects of other construction defects on the overall performance of the whole reinforced concrete structure.

V. References

[1] R. Zietsman, "Defects in the Construction Industry - Then and Now," in 5th Post Graduate Conference on Construction Industry Development, 2006, p. 108.

[2] A. Al-Hammad, S. Assaf, and M. Al-Shihah, "The effect of faulty design on building maintenance," Journal of Quality in Maintenance Engineering, vol. 3, pp. 29-39, 1997.

[2] ACI 301, "Specifications for Structural Concrete for Buildings," American Concrete Institute International, vol. 32, pp. 1313-2, 2005.

[3] ACI 503, "Proposed ACI Standard 503.4: Standard Specification for Repairing Concrete with Epoxy Mortars," in ACI Journal Proceedings, 1978.

[5] S. Bethmont, L. D'Aloia Schwartzentruber, C. Stefani, J. Tailhan, and P. Rossi, "Contribution of granular interactions to self-compacting concrete stability: Development of a new device," Cement and Concrete Research, vol. 39, pp. 30-35, 2009.

[6] S. A. Anagnostopoulos, "Inelastic beams for seismic analyses of structures," Journal of the Structural Division, vol. 107, pp. 1297-1311, 1981.

[7] F. Taucer, E. Spacone, F. C. Filippou, B. E. E. R. C. University of California, C. D. o. Transportation, and N. S. Foundation, A fiber beam-column element for seismic response analysis of reinforced concrete structures vol. 91: Earthquake Engineering Research Center, College of Engineering, University of California, 1991.

[8] T. Perea and R. Leon, "Composite Beam-Columns Performance Based on Nonlinear Fiber and Finite Element Analysis," 14WCEE. Beijing, China.

[9] R. Park, M. Priestley, and W. D. Gill, "Ductility of square confined concrete columns," Journal of the Structural Division ASCE, vol. 108, pp. 929-950, 1982.

[10] J. B. Mander, M. J. N. Priestley, and R. Park, "Observed Stress-Strain Behavior of Confined Concrete," Journal of structural engineering, vol. 114, pp. 1827-1849, 1988.

[11] S. A. Sheikh, "A comparative study of confinement models," ACI Journal, vol. 79, pp. 296-306, 1982.

[12] M. H. M. Yassin, "Nonlinear analysis of prestressed concrete sructures under monotonic and cyclic loads," University of California, Berkeley, 1994.

[13] B. Bousalem and N. Chikh, "Development of a confined model for rectangular ordinary reinforced concrete columns," Materials and structures, vol. 40, pp. 605-613, 2007.

[14] A. Gomes and J. Appleton, "Nonlinear cyclic stress-strain relationship of reinforcing bars including buckling," Engineering Structures, vol. 19, pp. 822-826, 1997.

[15] T. Albensi and C. Nuti, "Reinforcing Steel Bar Model," University Roma Tre, Rome, Italy, Department of Structures 2007.

[16] F. C. Filippou, E. P. Popov, and V. V. Bertero, "Effects of bond deterioration on hysteretic behavior of reinforced concrete joints," 1983.

[13] M. Berry, M. Parrish, and M. Eberhard, "PEER Structural Performance Database User's Manual (Version 1.0)," University of California, Berkeley, 2004.

[14] T. Ohno and T. Nishioka, "An experimental study on energy absorption capacity of columns in reinforced concrete structures," Proceedings of the JSCE, Structural Engineering/Earthquake Engineering, vol. 1, pp. 137-147, 1984.